Electronic states of AgCl nanocrystals embedded in crystalline KCl studied by 95-GHz optically detected magnetic resonance spectroscopy

G. Janssen, A. Bouwen, and E. Goovaerts
Department of Physics, University of Antwerp, Universiteitsplein 1, B-2610 Antwerpen, Belgium
(Received 29 July 2004; published 19 January 2005)

The properties of shallow electron centers (SEC), self-trapped holes (STH), and self-trapped excitons (STE) are investigated in nanocrystals of AgCl embedded in a crystalline KCl matrix. Time-resolved photoluminescence (PL) measurements reveal a behavior different from that in bulk AgCl: an inhomogeneous distribution of the properties of the recombination centers is revealed by the spectral dependence of the decay rates. In time scales from nano- to microseconds, slower rates are systematically observed at the low-energy side of the emission range. In high-frequency (95 GHz) optically detected magnetic resonance (ODMR) measurements, the transitions of SEC and STH centers are only observed in the extreme-low energy tail of the PL emission and they exhibit a broad and asymmetric g-value distribution (width $\delta g \approx 0.07$), ranging up from the respective bulk g-values. A complex behavior of the ODMR spectrum in the STE region is revealed, showing different spectra at 1.8 K and at higher temperature, and, different from the bulk AgCl case, exhibiting a strong dependence upon variation of the detection photon energy. Analysis of the measurements at 4.6 K yields a zero field splitting in the STE triplet state in good agreement with the bulk value, while the g-values are slightly increased relative to bulk, which is ascribed to the nanocrystal environment.

DOI: 10.1103/PhysRevB.71.035415 PACS number(s): 78.67.Bf, 73.21.La, 71.35.Aa, 76.70.Hb

I. INTRODUCTION

Due to their intermediate position between covalent semiconductors and ionic insulators and due to their importance as photosensitive materials, silver halides are of both fundamental and technological interest.[1,2] Being an indirect gap material, the effect of reduced dimensionality on the properties of AgCl crystals is of particular interest.

The luminescent properties of bulk AgCl single crystals have been investigated in detail in the past.[3–8] The photoluminescence (PL) of AgCl is characterized by a broad peak at 2.5 eV. Part of this PL originates directly from the recombination of excitons and is characterized by a decay with lifetimes in the microsecond ($\sim$10 μs) and the nanosecond ($\sim$1.5 ns) range. Also a nonexponential decay extending over 10 ms, which is due to the radiative recombination between distant electrons and holes, is contributing to this same luminescence band. A detailed microscopic picture of the electron and hole state in AgCl was obtained from the optical studies and from a wealth of electron paramagnetic resonance (EPR),[9–11] optically detected magnetic resonance (ODMR),[12–17] and electron nuclear double resonance (ENDOR)[18–20] investigations. These studies reveal that the hole is localized on a Ag^+ lattice ion as a self-trapped hole (STH, $g_\parallel = 2.147$ and $g_\perp = 2.040$), the hole-trapping being accompanied by a tetragonal Jahn-Teller distortion of the surrounding Cl^- ions. The resulting $AgCl_6^{4-}$ complex weakly binds an electron to form a self-trapped exciton (STE, $g_\parallel = 2.014$ and $g_\perp = 1.960$). In this STE, the electron is in a very diffuse hydrogenlike 1s orbital, while the hole is strongly localized. A shallowly trapped electron center (SEC, $g_{iso} = 1.881$) is formed when an electron is weakly bound to an intrinsic coulombic core or to impurity centers with an excess positive charge.[19]

Up to now, the effects of reduced dimensionality on electrons, holes and excitons in silver halides, has been most thoroughly studied in nanocrystals (NCs) of AgBr that are embedded in inverted micelles,[21,22] gelatin[22–24] or glass.[25] However, only when embedding such NCs in a crystalline matrix, they possess a well-defined orientation. In this way, AgBr NCs have been successfully embedded in a crystalline KBr matrix.[26,27] Also nanometer and micrometer sized AgCl crystals embedded in a crystalline KCl matrix have been successfully prepared as discussed in Refs. 28 and 29.

Vogelsang *et al.*,[28] have reported Q-band (36 GHz) ODMR measurements performed at 1.8 K on this type of AgCl NCs, showing strongly broadened STE-type resonance lines. Compared to the bulk AgCl parameters, changes in the STE g-values ($g_\parallel = 1.992$ and $g_\perp = 1.964$) and a decrease by a factor of 2 in the magnitude of the zero-field splitting ($D = -335$ MHz) were reported. Other Q-band studies on AgCl NCs,[29] report on a similar deviations of the STE parameters and on the presence of additional resonances that are ascribed to a STH with $g_\parallel = 2.016$ and $g_\perp = 1.974$.

As previously demonstrated for bulk AgCl, the increased resolving power at the W-band frequency of 95 GHz, compared to that at 36 GHz, allows for a more detailed investigation of the ODMR spectra and of the spin Hamiltonian parameters. In the present study, this approach is combined with an extensive photoluminescence-selective study of the ODMR spectra and with time-resolved measurements of the recombination luminescence, in order to investigate the SEC, STH, and STE centers in AgCl NCs embedded in a KCl single crystal matrix.

II. EXPERIMENT

Both continuous-wave and time-resolved PL measurements were performed in a liquid-helium-cooled optical cryostat at temperatures between 8 K and 12 K. Continuous-wave PL spectra were obtained using excitation with the

313 nm Hg line of a Mercury lamp. For the time-resolved PL measurements, laser pulses at 350 nm (3.54 eV) with a repetition time of 1.5 kHz and a pulse width of 2 ps were provided by a tunable laser system. The latter consists of an optical parametrical amplifier which is pumped by the pulses from a Ti:sapphire regenerative amplifier. A typical power of ~ 0.1 μW was used for the excitation of the crystal.

PL-intensity-detected ODMR measurements were performed at the *W*-band microwave frequency of 95 GHz with the sample centered within a split-coil 6 T superconducting magnet. For the low temperature (1.8 K) ODMR measurements an immersion cryostat and a custom–built Fabry-Perot cavity were used. The 4.5 K ODMR measurements were performed in a helium flow cryostat and a cylindrical cavity in combination with a special fiber bundel arrangement[30] to allow ODMR measurements. Similar results, but with a poorer signal to noise ratio, were found at this temperature of 4.5 K using the Fabry–Perot cavity (see Ref. 31). The crystal was continuously illuminated with the 350.7–356.4 nm multiline output of a Kr^+ laser with a typical incident power between 1 mW and 10 mW. The emission was collected through appropriate optical filters or a grating-monochromator onto an avalanche Si photodiode. Unless described differently, the microwave-induced changes in the PL intensity were synchronously detected with 336 Hz on–off modulation of the applied microwaves. All spectra were obtained using the maximum microwave power of about 1.5 mW on the sample.

III. AgCl/KCl CRYSTAL SPECIFICATIONS

The samples were grown in the Crystal Growth Facility of the Physics Department of the University of Paderborn (Germany) and are similar to the crystals described in Ref. 28. The AgCl nanocrystals (NCs) are formed in a Bridgman grown KCl single crystal by adding 2 mol % AgCl to the melt.

As KCl is transparent up to about 5.9 eV,[32] the formation of AgCl regions inside the crystal is shown by a PL emission at 2.35 eV—which is close to the PL band of bulk AgCl—after excitation with 3.96 eV light. The lattice symmetry axes of these AgCl crystals are oriented parallel to the axes of the surrounding KCl lattice. This is concluded from comparing the angular dependence of the *Q*-band[28] and our *W*-band ODMR spectra with the orientation of the KCl crystal axes. The latter are easily identified by the {100} cleavage planes of the sample.

Because the crystals are light sensitive, care was taken not to expose them to visible light (except for the AFM characterization) until they were cooled down to liquid helium temperatures. Changes of the luminescence and ODMR spectra after dark storage at room temperature for some months have been reported.[28,29] The crystals were therefore stored in a freezer at −21 °C for long storage times and in a refrigerator around 4 °C for shorter times. Over a period of 3 years no significant changes of the spectra were observed. Minor differences between measurements are most probably due to uncontrolled variations in applied laser and/or microwave intensities onto the samples.

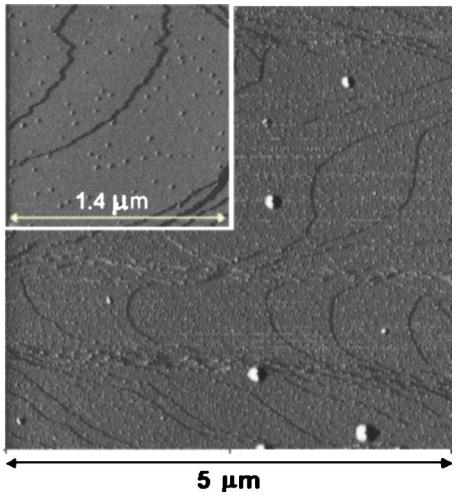

FIG. 1. AFM image (5 μm$\times 5$ μm) of a freshly cleaved surface of the KCl crystal containing AgCl particles. The presence of three AgCl particle sizes is illustrated in this image: the largest crystals (bump height $\sim$60 nm), a few particles with a height of $\sim$2–5 nm, and a very large number of small sized particles (bump height $\sim$0.5 nm). The latter are more clearly visible in the magnified part (1.4 μm$\times 1.4$ μm) in the inset. Note that the first derivative of the original AFM images is displayed here.

To gain insight into the AgCl particle sizes and distributions within the KCl matrix, several freshly cleaved crystal surfaces have been studied by means of atomic force microscopy (AFM). The AgCl particles reveal their presence by sticking out of the KCl matrix as is shown as an example in Fig. 1. Because the lateral size of these bumps is mostly determined by the diameter of the AFM tip—which has a radius of 5–10 nm—the height of the bumps is taken as a more representative measure for the particle sizes.[33] As illustrated in Fig. 1, the KCl matrix contains mainly three sizes of AgCl particles: a very large number of small crystallites sticking out of the matrix with a bump height of about 0.5 nm, a small amount of crystals showing bump heights between 2 and 5 nm, and some huge crystals with a height of approximately 60 nm. Inhomogeneities in the size distribution are observed, even within the same cleavage surface of the crystal: When moving the AFM tip over 1 to 2 mm, variations in density of the smallest particles are found of e.g. about 40 per 1 μm^2, towards no particles at all. Also the concentration of largest crystals varies considerable: Their concentration is highest in the rougher regions of the cleaved surface, indicating that they influence the cleavage. On average, an amount of about 3 large crystals is found per 5×5 μm^2.

IV. PROPERTIES OF THE AgCl PARTICLE PHOTOLUMINESCENCE

In the upper part of Fig. 2 the PL spectra from the AgCl crystals that are embedded in KCl and from a pure AgCl crystal are shown ($T=10$ K). The PL band of the AgCl particles is broadened by approximately 40% and its maximum, at 2.35 eV, is redshifted by about 120 meV compared to that

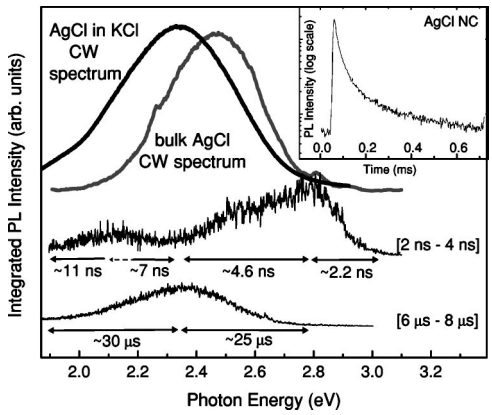

FIG. 2. Continuous-wave and time-selective PL spectra of the AgCl particles, obtained at $T=10$ K. For comparison, the CW spectrum of bulk AgCl is shown as well. The time behavior of the AgCl NC PL spectrum at ns and μs time scales, integrated over time windows after the laser pulse as indicated in the figure, is shown in the lower part. For each region in the PL spectrum, the corresponding decay times are indicated. Inset: Time decay of the total NC PL emission intensity (logarithmic scale), detected between 2.22 eV and 2.29 eV.

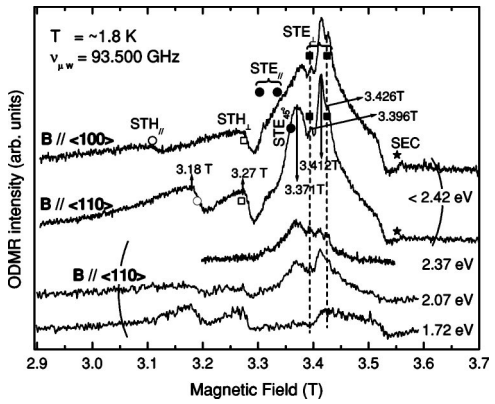

FIG. 3. Upper part: "Total" *W*-band (93.500 GHz) ODMR spectra at 1.8 K of the AgCl particles with $\mathbf{B}\|\langle 100\rangle$ and $\langle 110\rangle$, obtained by measuring changes in the entire PL-emission band. The expected field positions for STH, STE, and SEC in bulk AgCl are indicated in the figure for both field orientations. Lower part: Spectrally selective *W*-band ODMR spectra for $\mathbf{B}\|\langle 110\rangle$ measured at different detection photon energies using the appropriate interference filters, as is indicated in the figure.

of the bulk material. A similar change of the PL band was reported in Refs. 28 and 29 for AgCl NCs.

Similar to the photoluminescence from bulk AgCl, this PL-band of the AgCl particles is a superposition of an exponential decay with microseconds lifetime, a component in the nanosecond time range, and a nonexponential tail extending over milliseconds. The latter is illustrated in the inset of Fig. 2. The PL spectra, in a nanosecond time window after a short laser pulse, are considerably different from the total time-integrated spectrum, as illustrated in the middle curve of Fig. 2. Four PL bands can be distinguished. Below 2.1 eV a relatively slow exponential decay with $\tau \simeq 11$ ns is observed. This emission is overlapping with a band around 2.2 eV with an exponential decay of $\tau \simeq 7$ ns. Further, a PL band around 2.55 eV ($\tau \simeq 4.6$ ns) and a fast decay ($\tau \simeq 2.2$ ns) at 2.8 eV are present. Both in the microsecond and millisecond time range, the shape of the PL-spectra corresponds closely to the total time-integrated emission spectrum, but also in these longer time ranges, a dispersion of the decay kinetics is observed: In each case there is an increase of the decay times at decreasing PL emission energies (see bottom spectrum in Fig. 2 and Ref. 28 for the two time-ranges, respectively).

This dispersion in the decay times is a particular feature of the AgCl/KCl crystal, and it can be attributed to the size distribution of the AgCl particles. Indeed, in contrast with our findings for the AgCl particles, the line position and shape of the bulk AgCl PL band was found to be independent of time and identical to the continuous-wave PL band both in the nanosecond (starting from 0.6 ns)[7] as well as the microsecond[6] time range.

V. *W*-BAND ODMR MEASUREMENTS

To examine the effects of size reduction on electron, hole and exciton states in the AgCl particles, the contributions to the luminescence band are further studied by *W*-band ODMR spectroscopy.

A. Low temperature—1.8 K—ODMR measurements

In the upper part of Fig. 3 representative *W*-band spectra from the AgCl/KCl crystal are shown, measured at $T=1.8$ K for two magnetic field orientations relative to the crystal lattice ($\mathbf{B}\|\langle 100\rangle$ and $\langle 110\rangle$). These spectra were obtained by monitoring the microwave-induced changes of the entire PL band and they are therefore called the "total" ODMR spectra. With a cut-off filter at 420 nm, the emission above 2.95 eV is blocked. The same spectra, with improved signal-to-noise ratio are obtained when using a cut-off filter of 513 nm (transmission below 2.42 eV). Compared to the bulk AgCl ODMR spectra, additional resonances are observed and all lines are considerably broadened. Whereas the photon energy of the PL detection does not influence the relative intensities or the shape of the resonance lines in the bulk material,[34] a strong spectral dependence of the ODMR spectra is observed for the AgCl/KCl sample. This is illustrated in the lower part of Fig. 3 in which we present the spectra measured along the $\langle 110\rangle$ direction at different photodetection energies by using the appropriate interference filters.

The broad and highly asymmetric low-field resonances (at 3.18 T and 3.27 T for $\mathbf{B}\|\langle 110\rangle$) originate from centers emitting at a photon energy below 2.07 eV, which is the far low-energy tail of the PL band. Their field positions correspond to the expected resonances from the STH in pure AgCl with $g_{\|}^{h}=2.147$ and $g_{\perp}^{h}=2.040$. An angular variation from $\mathbf{B}\|\langle 100\rangle$ towards the $\langle 110\rangle$ direction (see Fig. 4), confirms this assignment to an $S=1/2$ center with the bulk STH g-values. Associated with these STH resonances, there is a very wide band with sharp edges between 3.40 T and 3.53 T, which is in the region between the bulk SEC g-value ($g=1.881$) and the free

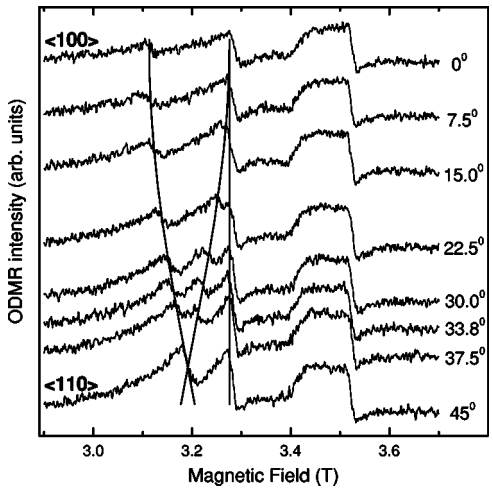

FIG. 4. *W*-band (93.535 GHz) ODMR angular variation of the AgCl particles at 1.8 K. A 715 nm cut-off filter is used to obtain changes in the PL below 1.73 eV. A simulation of the angular variation of the STH is indicated, using the bulk AgCl parameters $g_{\parallel}^{h}=2.147$ and $g_{\perp}^{h}=2.040$.

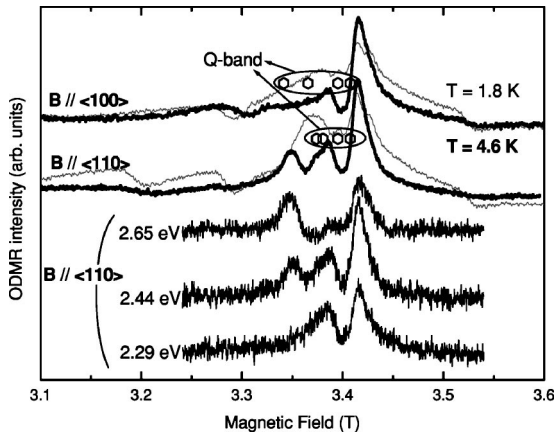

FIG. 5. Upper part: "Total" *W*-band (93.500 GHz) ODMR spectra at 4.6 K of the AgCl particles for $\mathbf{B}\|\langle 100\rangle$ and $\langle 110\rangle$. The spectra were obtained using a cut-off filter of 475 nm. As a reference, the spectra obtained at 1.8 K are shown in gray. The circles represent the calculated resonance positions using the parameters for the STE derived from the *Q*-band measurements reported in Ref. 28. Lower part: Spectrally selective ODMR spectra for $\mathbf{B}\|\langle 110\rangle$ measured at different detection photon energies as indicated in the figure. The detection energies are selected using a grating-monochromator, with a bandwidth of $\simeq$60 meV.

electron g-value at $g\simeq 2$ (see bottom spectrum in Fig. 3 and Fig. 4). The shape and the position of this band remain unchanged upon rotating the static magnetic field direction. This broad band is correlated with the resonances assigned to the STH in AgCl, as demonstrated by their similar dependence on the emitted PL energy (both resonances originate from the extreme low-energy tail of the PL band), and also by their analogous dependence on the modulation frequency. Indeed, the intensity of both these resonances increases when detecting with lower modulation frequencies, which is not the case for the other resonance lines. We are associating this band with SEC centers inside the AgCl particles. This assignment and its correlation with the STH resonances will be further discussed in Sec. VI.

As shown in Fig. 3, a sharp feature is also observed close to the expected position of the SEC resonance line in bulk AgCl at $g=1.881$ (3.551 T). This feature is associated with SECs in the relatively large AgCl regions with properties of the bulk material.

Because of the width of the resonance lines between 3.30 T and 3.52 T, an angular variation from $\mathbf{B}\|\langle 100\rangle$ towards the $\langle 110\rangle$ direction does not univocally reveal the nature of the different lines in this region. Considering the isotropic nature and the line positions of the weak and narrow peaks at 3.396 T and 3.426 T (see Fig. 3), these resonances are assigned to the perpendicular components of the STE in bulk AgCl, characterized by $g_{\perp}^{\mathrm{STE}}=1.960$. In agreement with this assignment, these resonances originate from centers emitting between 2.2 eV and 2.7 eV (see Fig. 3, in particular the spectrum measured with a PL detection of 2.37 eV), which corresponds to the PL band of bulk AgCl. Note that the presence of the STE_{45° line is not clear from the spectra, probably because of the superposition with intense NC-related signals.

Another set of intense lines is observed in the ODMR spectrum in Fig. 3 at 3.371 T and 3.412 T for $\mathbf{B}\|\langle 110\rangle$. These lines originate from centers emitting at lower energies (maximum emission around 2.2 eV) than the bulklike centers described above. As will be discussed in the following, it is likely that they are related to STEs with a more NC-like character. It should be noted that the 3.371 T peak exhibits a maximum ODMR intensity when detecting at an energy of 2.28 eV, while the maximum of the 3.412 T peak is observed when detecting the ODMR spectrum at 2.10 eV.

Besides the changes observed by variation of the microwave modulation frequency, also the power of the microwaves in the cavity and the laser excitation intensity have an influence on the shape of the ODMR spectra. At low excitation and/or microwave power, the broad STH signals are favored, while the other resonance lines increase when applying higher powers.

B. "High" temperature—4.6 K—ODMR measurements

Considerable changes in the ODMR spectra are observed when measuring at temperatures around 4.6 K. In Fig. 5, *W*-band ODMR spectra, obtained in the cylindrical cavity at 4.6 K, are presented and compared to the corresponding spectra at 1.8 K.

The sharp features at 3.396 T and 3.426 T which were clearly observable at 1.8 K (see Fig. 3) and which were assigned to resonances from bulklike STE AgCl centers, are no longer observable at 4.6 K. Parallel to the disappearance of the bulk STE resonances at higher temperature, there is a drastic decrease in intensity of the STH lines, which, at this temperature, are only observable under optimal conditions. Preliminary 4.8 K *W*-band ODMR measurements obtained using the Fabry–Perot cavity (see Janssen *et al.*[31]), did not reveal the presence of these STH resonances. The spectra presented here illustrate the improved signal to noise ratio achievable in the cylindrical cavity.[30] As in the case of the

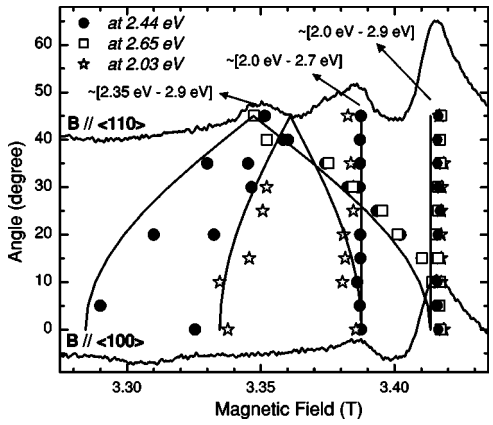

FIG. 6. Cumulative orientational dependence of the ODMR lines (93.50 GHz) at 4.6 K from emission-selective measurements. The detection energy is specified in the figure by circles (2.44 eV), squares (2.56 eV), and stars (2.03 eV). A simulation is plotted of the angular variation of an $S=1$ system with $g_{\perp}=1.965$, $g_{\parallel}=2.018$, and $|D|=710$ MHz from the $\langle 100\rangle$ direction at $\theta=0°$ to the $\langle 110\rangle$ direction at $\theta=45°$.

low-temperature measurements, the STH lines and the broad SEC band could be enhanced by applying lower modulation frequencies.

Similar to the observations at 1.8 K, there is a clear dependence of the ODMR spectra on the emission energy, as shown in the lower part of Fig. 5 for the $\langle 110\rangle$ spectrum. Three different resonance lines can be distinguished, each of them exhibiting a different dependence on the photodetection energy. The same energy-regions are observed in the PL spectrum of the NCs in the nanosecond time-range after the laser pulse (see Fig. 2). The ODMR line at 3.347 T, originates from an emission in the PL band between 2.43 eV and 2.95 eV which corresponds to centers having the shortest PL decay components. The resonance at 3.385 T is only clearly visible at a detection energy between 1.97 eV and 2.64 eV (longer lifetimes) and the 3.416 T peak is observable over almost the complete spectral range of the PL band (1.97 eV–2.95 eV). No direct correlation is found between these resonance lines observed at 4.6 K and the ones measured at 1.8 K.

An extensive angular study of the emission-selective ODMR spectra was performed and the line positions gathered at these different PL photon energies are summarized in Fig. 6. The full lines represent the orientational dependence expected from the following spin Hamiltonian for $S=1$:

$$\mathcal{H}=\mu_B \mathbf{B}_0 \cdot \overleftrightarrow{g} \cdot \mathbf{S} + D\left[S_z^2 - \tfrac{1}{3}S(S+1)\right].$$

The bulk AgCl STE value of the zero field splitting parameter ($|D|=710$ MHz) and only slightly higher g-values ($g_{\parallel}=2.018(3), g_{\perp}=1.965(1)$) were used for the simulation. This g-shift of +0.004 units compared to the bulk STE g-values ($g_{\parallel}=2.014, g_{\perp}=1.960$),[16] is larger than the error margin and is a property of the NCs. Considering the large linewidth and combining the STE-type resonances for all of the PL detection energies, the field positions are well reproduced using these parameters. Note that, due to their weak intensities, there is a large error in the field positions of the low-field lines, belonging to the parallel component of the spectrum. The splitting between singlet and triplet states due to the electron–hole exchange interaction ($J \simeq -5$ cm^{-1}) was not considered for this simulation. Taking into account this interaction, would however further improve the correspondence between the simulated and the measured field positions.[16]

VI. DISCUSSION AND INTERPRETATION

The broadening of the ODMR resonance lines compared to those from bulk AgCl, at 1.8 K as well as at 4.6 K, is correlated with a distribution in the sizes of the AgCl particles and in the positions of the recombination centers inside these crystals.

Considering their line positions, their isotropic nature and the dependence on PL detection energy, the weak peaks at 3.396 T and 3.426 T, observed at 1.8 K (see Fig. 3), are assigned to the $STE_{\perp}$ transitions in bulk AgCl. They originate from STE transitions in larger regions of AgCl, possessing near to bulk properties. The presence of such larger AgCl regions is confirmed by the AFM measurements, which revealed a small number of large (height 60 nm) AgCl crystals. The $STE_{\parallel}$ lines probably escape detection due to their even smaller intensity and the overlap with other spectra. Also the sharp feature around $g=1.881$, assigned to SECs in bulk AgCl, is associated with these larger regions of AgCl in the crystal.

A large g-value distribution is found for the resonances associated to SEC and STH centers: In each case there is a broadening towards higher g-values from the bulk value at the high field edge. The broad and isotropic band is assigned to shallow electron traps at low temperature. The corresponding g-values range between $g=1.96$ and 1.89, which is between the field position of the SEC in bulk AgCl and the free electron g-value. The asymmetrically broadened lines, assigned to the STH resonances, have a minimum g-value corresponding to that of the bulk STH ($g_{\parallel}=2.147, g_{\perp}=2.040$). The line broadening corresponds to a g-variation of ≈ 0.07, which is comparable with the spread of g-values observed for the SEC band. The width of these SEC and STH resonances is ascribed to a distribution of different binding energies of the corresponding centers, yielding the distribution in g-values. This variation most probably results from the distribution in NC sizes (and thus of the strain on these NCs) and the possible variation of the positions of the STH and SEC centers within the NCs. The bulklike g-values are obtained for centers that are positioned in the middle of the larger NCs; all other locations give rise to the higher values.

While bulk AgCl has a uniform emission at 2.5 eV, the recombination of STH and SEC in the NCs gives rise to an emission below 2.07 eV, which is the far low energy-edge of the NC emission band. This is—tentatively—explained in the following way: Near the interface between AgCl NCs and KCl matrix band, bending of the conduction and valence bands can occur, due to the difference in materials properties,

the strain induced by lattice matching and possible space charges due to defects. The changes in band energy between the positions of STH and SEC have to be added to the expected energy difference and can result in emission of this tunneling recombination at lower energy than observed in bulk AgCl. The recombination energy of the STE, with bound electron–hole pair in closely the same position, is not influenced as such by the band-bending, and its emission remains close to that in bulk AgCl.

The influence of the modulation frequency on both STH and SEC resonances is in agreement with the relatively longer radiative lifetime of these centers. The increased intensity of these lines at lower temperature is explained as a more efficient binding of the electron to shallow traps at low temperature. At increasing temperatures, the electron will more easily move from the shallow trap to a STH to form a STE.

The remaining resonances observed in the 1.8 K ODMR spectra (in Fig. 3 at 3.371 T and 3.412 T for $\mathbf{B}\|\langle 110\rangle$) are assigned to STE centers confined in the smaller NCs or more to the edge of the larger crystals, where strain-effects alter their properties compared to the bulk centers. This assignment is derived from considering their field positions and their PL detection energy dependence, which in each case are close to that of the bulk STE centers.

The difference of these STE-like resonances observed at 1.8 K with the resonances composing the STE-like angular variation in Fig. 6 at 4.6 K is not explained at this point. At low temperature, an increased intensity of the resonances from impurities like Br^- is expected in the spectrum of AgCl crystals.[35,36] The differences between the STE-like ODMR spectra at 1.8 K and 4.6 K might be induced by these impurities. However, an impurity exclusion effect, which has been observed in small AgBr crystals,[37,38] is also expected in these AgCl NCs. Since the simulation using near-to-bulk like STE parameters is reproducing the field positions at 4.6 K fairly well, also these resonances observed at 4.6 K are assigned to such STE centers. It is peculiar that the different resonance lines composing this angular variation are observed at a different PL detection energy. One can assume either that the different resonance lines are obtained from different centers, each giving rise to another ODMR active line. Alternatively, all resonances would originate from the same centers, but different excited states are detected. Note also that there is a clear correspondence between these energy regions and the energy bands observed in the nanosecond time scale.

The high complexity of the system with AgCl nanoparticles embedded in KCl, as derived from our *W*-band study, is in contrast with the simpler picture derived previously from *Q*-band measurements.[28,29] Both the application of higher microwave frequencies and the more extensive study of the spectral dependence of the ODMR spectra have clarified this aspect of the AgCl NC system.

The *Q*-band spectra reported in Ref. 28 were obtained at 1.8 K by monitoring energies between 2.29 eV and 2.48 eV. As is shown with our *W*-band study, the resonances from the STH and the SEC in the NCs can not be observed at this detection energy. Baranov *et al.*[29] also did not report about these STH and SEC-like resonances. The growth procedure of the crystals examined in this investigation may be somewhat different, which may be at the origin of such differences. However, it is not clear from this report whether an extensive examination was performed of the spectrum at the corresponding lower detection energies.

When fitting the parameters derived from the *Q*-band data ($g_\parallel = 1.992$, $g_\perp = 1.964$, and $|D| = 335$ MHz)[28] to our 93.500 GHz spectra (see Fig. 5), no correspondence is found with the *W*-band resonance lines. Differences in both the PL and the ODMR spectra can be expected between differently grown AgCl/KCl crystals. The AgCl/KCl crystal described in this article is however obtained from the same growth procedure as was described in Ref. 28. In addition the PL spectra of both crystals are the same. The PL detection energy and the temperature of the *Q*-band measurements were optimum for detecting the bulklike resonances. The central line at 1.34 T in the *Q*-band spectra in Ref. 28 are therefore ascribed, not to a resonance from the NCs, but to a bulk $STE_\perp$ resonance line, in agreement with its field position.

Note that Ref. 29 reports on an $S=1/2$ center which is attributed as originating from a STH center with $g_\parallel = 2.016$ and $g_\perp = 1.974$. We do not find any evidence for the presence of this $S=1/2$ center.

VII. CONCLUSIONS

The emission from the AgCl NCs exhibits a time behavior significantly different from that in bulk AgCl. Longer radiative lifetimes are observed at the low-energy edge of the NC PL band and the spectrum at the nanosecond timescale is considerable different from the CW and time-integrated spectrum.

By using the high microwave frequency of 95 GHz and performing an accurate spectral analysis of the ODMR spectra, the high complexity of this system of AgCl NCs grown in a KCl matrix was further unravelled. Whereas the ODMR spectrum of bulk AgCl is independent of the PL detection energy, a large dependence on the PL detection energy was observed for this crystal. The resonances associated to SEC and STH centers are highly broadened. The large *g*-value distribution of these lines ranges from the bulk value upwards. Furthermore, these resonances were observed only for detection in the extreme-low energy edge of the PL emission and their relative line intensities increased substantially at lower temperature and at lower modulation frequency.

For the STE centers also, the measurements reveal the reduced size effects in the NCs: The STE region of the ODMR spectrum shows strongly broadened lines compared to the bulk AgCl spectra, and moreover different spectra when cooling to the lowest temperature ($T = 1.8$ K) compared to the higher temperature region ($T > 4.2$ K). The complexity of the spectra was further evidenced when measuring their dependence on the detection photon energy. Combining the transitions detected in three spectral regions of the STE-type emission yields an overall angular variation corresponding closely to that of the STE in bulk AgCl. In this analysis the zero-field splitting is unchanged relative to the bulk value, but the *g*-values are slightly but significantly increased in the AgCl in KCl NCs.

ACKNOWLEDGMENTS

This work was supported financially by the National Fund for Scientific Research (FWO-Flanders, group research project G.0409.02). We are very grateful to Wolf von der Osten from the Department of Physics, University of Paderborn (Germany) for supplying samples and for discussions. We also gratefully acknowledge D. M. Bruls and P. M. Koenraad from the Technical University of Eindhoven (The Netherlands) for the AFM characterization of the samples.

[1] T. H. James, *The Theory of the Photographic Process* (Macmillan, New York, 1977).
[2] A. P. Marchetti and R. S. Eachus, Adv. Photochem. **17**, 145 (1992).
[3] G. C. Smith, Phys. Rev. **140**, A221 (1965).
[4] H. Kanzaki, S. Sakugari, and K. Sakamoto, Solid State Commun. **9**, 999 (1971).
[5] M. Tsukakoshi and H. Kanzaki, J. Phys. Soc. Jpn. **30**, 1423 (1971).
[6] M. S. Burberry and A. P. Marchetti, Phys. Rev. B **32**, 1192 (1985).
[7] H. Liu, R. T. Williams, G. P. Williams, L. M. Slifkin, and C. Childs, *Defects in Insulating Materials*, edited by J. M. Speath and O. Kanert (World Scientific Publishing Co., Singapore, 1992), p. 1048.
[8] L. G. Grigorjeva, E. A. Kotomin, D. K. Millers, and R. I. Eglitis, J. Phys.: Condens. Matter **7**, 1483 (1995).
[9] M. Höhne and M. Stasiw, Phys. Status Solidi **28**, 247 (1968).
[10] C. L. Marquadt, R. T. Williams, and M. N. Kabler, Solid State Commun. **9**, 2285 (1971).
[11] E. Laredo, W. B. Paul, L. Rowan, and L. Slifkin, Phys. Rev. B **27**, 2470 (1983).
[12] W. Hayes, I. B. Owen, and P. J. Walker, J. Phys. C **10**, 1751 (1977).
[13] A. P. Marchetti and D. S. Tinti, Phys. Rev. B **24**, 7361 (1981).
[14] M. Yamaga, N. Sugimoto, and H. Yoshioka, J. Phys. Soc. Jpn. **54**, 4340 (1985).
[15] J. P. Spoonhower, F. J. Ahlers, R. S. Eachus, and W. G. McDugle, J. Phys.: Condens. Matter **2**, 3021 (1990).
[16] M. C. J. M. Donckers, O. G. Poluektov, J. Schmidt, and P. G. Baranov, Phys. Rev. B **45**, 13 061 (1992).
[17] O. G. Poluektov, M. C. J. M. Donckers, P. G. Baranov, and J. Schmidt, Phys. Rev. B **47**, 10 226 (1993).
[18] M. T. Bennebroek, A. Arnold, O. G. Poluektov, P. G. Baranov, and J. Schmidt, Phys. Rev. B **53**, 15 607 (1996).
[19] M. T. Bennebroek, A. Arnold, O. G. Poluektov, P. G. Baranov, and J. Schmidt, Phys. Rev. B **54**, 11 276 (1996).
[20] M. T. Bennebroek, A. v. Duijn-Arnold, J. Schmidt, O. G. Poluektov, and P. G. Baranov, Phys. Rev. B **66**, 054305 (2002).
[21] H. Stolz, H. Vogelsang, and W. von der Osten, in *Handbook of Optical Properties: Optics of Small Particles, Interfaces and Surfaces*, edited by R. E. Hummel and P. Wissmann (CRC Press, Boca Raton, 1997), Vol. II, p. 31.
[22] A. P. Marchetti, K. P. Johansson, and G. L. McLendon, Phys. Rev. B **47**, 4268 (1993).
[23] H. Kanzaki and Y. Tadakuma, Solid State Commun. **80**, 33 (1991).
[24] Y. Masumoto, T. Kawamura, T. Ohzeki, and S. Urabe, Phys. Rev. B **46**, 1827 (1992).
[25] A. P. Marchetti, P. J. Rodney, and W. von der Osten, Phys. Rev. B **64**, 132201 (2001).
[26] H. Vogelsang, PhD thesis, University of Paderborn, 1999.
[27] P. G. Baranov, N. G. Romanov, V. L. Preobrazhenskii, and V. A. Khramtsov, JETP Lett. **76**, 465 (2002).
[28] H. Vogelsang, O. Husberg, U. Kohler, W. von der Osten, and A. P. Marchetti, Phys. Rev. B **61**, 1847 (2000).
[29] P. G. Baranov, N. G. Romanov, V. A. Khramtsov, and V. S. Vikhnin, J. Phys.: Condens. Matter **13**, 2654 (2001).
[30] G. Janssen, A. Bouwen, P. Casteels, and E. Goovaerts, Rev. Sci. Instrum. **72**, 4295 (2001).
[31] G. Janssen, E. Goovaerts, S. V. Nistor, A. Bouwen, D. Schoemaker, H. Vogelsang, and W. von der Osten, Radiat. Eff. Defects Solids **156**, 141 (2001).
[32] *American Institute of Physics Handbook*, edited by D. E. Gray (McGraw-Hill Book, New York, 1972).
[33] The true crystal size is different from the measured bump height because the AgCl particles stick out of the KCl matrix with different parts of their volume. Further, the AFM measurements were performed at room temperature, in normal atmosphere and under visible light, which might also have somewhat affected the measured heights. The obtained heights can however be considered to be indicative for the NC sizes.
[34] This was examined with the same ODMR setup. Data not shown.
[35] M. Yamaga, N. Sugimoto, and H. Yoshioka, J. Phys. Soc. Jpn. **54**, 4340 (1985).
[36] J. P. Spoonhower, F. J. Ahlers, R. S. Eachus, and W. G. McDugle, J. Phys.: Condens. Matter **2**, 3021 (1990).
[37] H. Kanzaki and Y. Tadakuma, Solid State Commun. **80**, 33 (1991).
[38] H. Vogelsang and W. von der Osten, *Excitonic Processes in Condensed Matter*, edited by R. T. Williams and W. M. Yen (The Electrochemical Society, Pennington, 1998), Vol. 25, p. 240.